First principles study of the structural, electronic, optical and thermal properties of chalcopyrite semiconductor $LiAlTe_2$

© H. Benkhedim[1,2], H. Meradji[1], S. Ghemid[1], A. Bouasla[2], A. Boumaza[1]
H. Bendjeddou[1], Z. Chouahda[1], R. Khenata[3]

[1] Laboratoire LPR, Département de Physique, Faculté des Sciences, Université Badji Mokhtar, Annaba, Algeria
[2] Laboratoire des Semi-conducteurs, Département de Physique, Faculté des Sciences, Université Badji Mokhtar, Annaba, Algeria
[3] Laboratoire de Physique Quantique de la Matiére et de la Modélisation Mathématique (LPQ3M), Université de Mascara, Mascara, 29000, Algeria

E-mail: hmeradji@yahoo.fr

Received February 24, 2021
Revised October 28, 2021
Accepted for publication May 16, 2022

The structural, electronic, optical and thermal properties of chalcopyrite $LiAlTe_2$ are studied using the full potential linearized augmented plane wave (FP-LAPW) method framed within density functional theory (DFT). The Wu-Cohen generalized gradient approximation (WC-GGA) was used as exchange-correlation potential to calculate the structural properties. Furthermore, the Tran and Blaha modified Becke-Johnson (mBJ) functional was also employed to compute the electronic and optical properties in order to get best values. The structural parameters at equilibrium are in good agreement with previous experimental and theoretical calculations. The band structures and density of states are calculated and it is found that $LiAlTe_2$ compound is a direct band gap (Γ-Γ) semiconductor. In addition, the optical properties such as dielectric function, refractive index, reflectivity and absorption coefficient are calculated for photon energies up to 25 eV. This study on the optical properties has also been enriched by the introduction of the analysis of birefringence and anisotropy for this material. The calculated values of all parameters are compared with the available theoretical data where a reasonable agreement has been obtained. The study of the material properties at high temperatures and pressures is very important to understand the behavior of a material in severe conditions, so the temperature and pressure dependencies of unit cell volume, bulk modulus, Debye temperature and specific heat capacities are obtained at different temperatures ($0-1000$ K) and pressures ($0-8$ GPa) using the quasi-harmonic Debye model. To our knowledge this is the first theoretical prediction of the thermal properties for $LiAlTe_2$ compound and still awaits experimental confirmations. We have included the spin-orbit interaction (SOI) in our calculations which is known to have significant influence on the electronic and optical properties when heavy elements are present. A weak effect is observed for the studied compound.

Keywords: DFT, Wien2k, Chalcopyrite, band gap, dielectric function, thermal properties.

DOI: 10.21883/SC.2022.08.54118.9597a

1. Introduction

Chalcopyrite crystals are of considerable interest because of their potential applications in optoelectronic devices such as light emitting diodes and laser diodes operating in the blue and ultraviolet wavelength region. This is due to their direct band gap and birefringent nature [1–4]. Ternary chalcogenides with the general formula $A^IB^{III}C_2$ (A = Li, Na, Cu, Ag; B = Al, Ga, In; C = S, Se, Te) have attracted considerable attention due to their uses as solar energy converters, nonlinear optical (NLO) devices, light emitting diodes (LED), and detectors [5–7]. These materials crystallize in the chalcopyrite structure with the space group $I\bar{4}2d$. The chalcopyrite structure is a superlattice of the cubic zinc-blende structure. It may be obtained from the zinc-blende structure by ordering the two cation sublattices. The majority studies are performed on compounds containing Cu or Ag as monovalent cation, very less literature is available for ternary lithium chalcogenides; possibly because of crystal development adversities and air sensitivity of this class of compounds. Ternary Li-containing chalcogenides $LiMX_2$ (M = Al, Ga, In; X = S, Se, Te) are promising materials, they could be developed as thin films making them important for solar panel applications [8]. Also, these $LiMX_2$ compounds attracted considerable attention due to their potential applications in solar cells [9], light-emitting diodes [10], and nonlinear optical devices [11] along with optical frequency conversion applications in solid state tunable laser systems [12]. Motivated by the above considerations, $LiAlTe_2$ belonging to the $LiMX_2$ compounds is investigated in the present study. $LiAlTe_2$ compound was synthesized for the first time by Kim *et al* [5] who studied its electronic structure; two crystalline modifications were determined: (a) with space group and (b) with space group P3m1 (№ 156). Kosobutsky *et al* reported ab-initio calculations of the phonon dispersion curves and the elastic constants of this compound [13]. Kosobutsky and Basalaev [14] have performed the electronic and optical

properties of $LiMTe_2$ (M = Al, Ga, In) compounds in the chalcopyrite structure. The structural, electronic and optical properties of $LiAlTe_2$ have been investigated by Amjad Khan *et al* [8]. Electronic structure, electronic charge density, linear and nonlinear optical properties of single crystal α-$LiAlTe_2$ has been investigated using full-potential augmented plane wave method (FP-LAPW) of the density functional theory [15]. However, among $LiMTe_2$ (M = Al, Ga, In) compounds, sufficiently detailed experimental studies of the optical properties in the IR range have been performed only for $LiGaTe_2$ [16,17], while for $LiAlTe_2$ and $LiInTe_2$ there is very limited information on their physical properties in the literature. In the present manuscript, we have aimed to provide some additional information to the existing data on the physical properties of $LiAlTe_2$ compound by using the full-potential linearized augmented plane wave method (FP-LAPW) within the framework of the density functional theory (DFT). The rest of the paper is as follows: in section 2, we briefly describe the computational techniques used in this study. In Section 3, the main results are presented and discussed. Finally, in Section 4, we concluded our results.

2. Computational details

All the computations in the present study are performed with the full-potential linearized augmented plane wave method (FP-LAPW) [18] within the framework of density functional theory (DFT) [19,20], as implemented in WIEN2K code [21]. The Wu-Cohen (WC) functional under generalized gradient approximation (GGA) was used to treat the exchange and correlation effects [22]. Additionally, The modified Becke–Johnson potential (mBJ) exchange potential approximation [23,24] was also used for the studies of electronic and optical properties. It is a modified version of potential introduced by Becke-Johnson [24] to improve the band gaps calculated by DFT. In the FP-LAPW method, the wave function, charge density and potential were expanded by spherical harmonic functions inside non-overlapping spheres surrounding the atomic sites (muffin-tin spheres) and by plane-waves basis set in the remaining space of the unit cell (interstitial region). To separate core states from valence states, the cut-off energy is set to -6Ry. The maximal l value for the wave function expansion inside the atomic spheres was confined to $l_{\max} = 10$ while the charge density was Fourier expanded up to $G_{\max} = 12(\text{Ry.})^{1/2}$, where $G_{\max}$ is the largest vector in the Fourier expansion. The cut-off energy for plane wave expansion of wave functions in the interstitial region is taken to be $K_{\max} = 8/R_{MT}$, where R_{MT} is the smallest muffin-tin radius. The values 1.93, 2.17, 2.5 a.u. have been chosen as the R_{MT} of Li, Al and Te atoms, respectively. The Brillouin zone (BZ) was sampled at 40 special k-points generated using $7 \times 7 \times 7$ Monkhorst–Pack meshes [25]. The self-consistent calculations are converged up to 10^{-4}Ry. The spin-orbit interaction is added using second variation method programmed in the code WIEN2K.

3. Results and discussions

3.1. Structural properties

In chalcopyrite structure of $I\bar{4}2d$ space group, Li, Al and Te atoms are located at Wyckoff positions 4a (0, 0, 0), 4c (0.5, 0.5, 0), and 8d (u, 0.25, 0.125), respectively, where u is an internal parameter denoting the dimensionless anion displacement. The unit cell of $LiAlTe_2$ is shown in Fig. 1. The tetrahedron is distorted along the crystal c-axis, giving rise to deviation of the c/a ratio and the internal parameter u from their ideal values of 2.0 and 0.25. Thus, the cell energy depends on three geometrical parameters: $E = E(a, c, u)$. The total energy is calculated in two steps. First, we have calculated the energy at different volumes, keeping c/a constant. In the second step, the c/a ratio is optimized by calculating c/a versus energy, keeping the volume fixed at its minimal value. The internal parameter u is minimized by calculating the internal forces acting on the atoms within the unit cell until the forces become negligible by using the MINI program included in the WIEN2K code. The ground state properties of interested compound are obtained by fitting the calculated energy versus volume curves to Murnaghan's equation of state [26]. Fig. 2 shows the calculated total energy as a function of volume for $LiAlTe_2$ compound. The structural parameters such as lattice constants (a and c), bulk modulus (B) and its pressure derivative (B') are listed in Table 1 along with other available theoretical results and experimental data. Our results show that the obtained lattice parameter a is

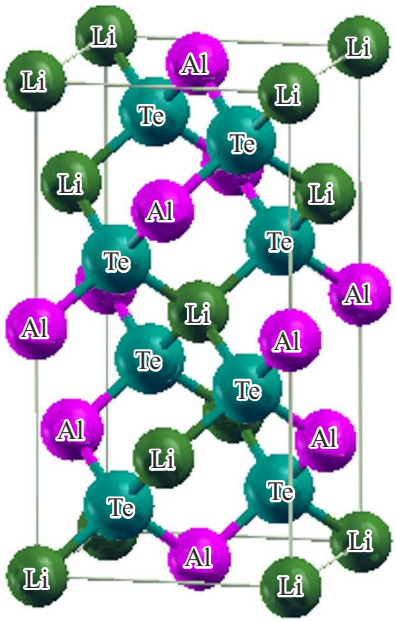

Figure 1. Crystal structure of chalcopyrite $LiAlTe_2$.

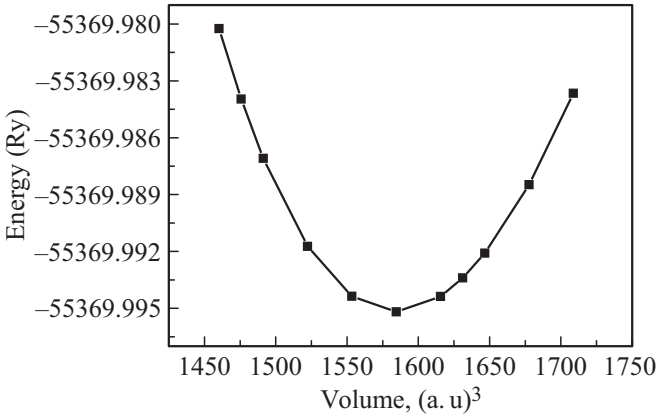

Figure 2. Variation of energy as a function of volume for $LiAlTe_2$ compound.

1.44% less than the experimental value [27], on the other hand the lattice parameter c is 2.43% higher than that of experiment [27]. Otherwise, our results are in reasonable agreement with available theoretical ones [8,13]. For the bulk modulus, our obtained value agrees with that in Ref [8]. However we note the lack of experimental and theoretical values of the pressure derivative of the bulk modulus. The bulk modulus provides information about crystal rigidity and large bulk modulus indicates high crystal rigidity. It is noted from Table 1 that the studied compound has relatively low bulk modulus value and therefore, it has high compressibility and low hardness.

3.2. Electronic properties

The electronic properties of $LiAlTe_2$ compound are analyzed by calculating band structures and the total and partial density of states (DOS). Using the lattice constants obtained with WC-GGA, we have calculated the band structures along the high symmetry directions in the first Brillouin zone using both WC-GGA and mBJ schemes. The band structure profiles obtained by the mBJ and the WC-GGA approximations are similar and the difference occurs essentially in the band gap values. The calculated band structures of this compound are presented in Fig. 3 (WC-GGA (a), mBJ (b)). It is seen from the plots that $LiAlTe_2$ is found to be direct-band gap semi-conductor, the valence band maximum (VBM) and the conduction band minimum (CBM) are both located at the Γ-point. The valence band consists of three groups of bands, as in the majority of crystals belonging to the chalcopyrite family. The calculated band gap values within WC-GGA and mBJ are displayed in Table 2 along with other theoretical calculations. The band gap value obtained by mBJ is in good agreement with that predicted by Reshak *et al* [15]. One can expected that the band gap predicted in this work using mBJ is more realistic than those obtained by WC-GGA, since mBJ exchange-correlation potential provides band gap values which usually are very close to the experimental

Table 1. Calculated structural equilibrium parameters (a, c, u), bulk modulus (B) and the pressure derivative of the bulk modulus (B') of $LiAlTe_2$ using WC-GGA approximation

a (Å)	c (Å)	u	B (GPa)	B'	Reference
6.259	11.976	0.260	38.967	4.386	This work
6.351	11.691				[27] expt
6.242	11.643	0.2614			[13]
6.455	11.882	0.229	40.93		[8]

Table 2. Calculated band gap of $LiAlTe_2$ compared to the available theoretical data

Band gap (eV)	Used approximation	Reference
2.159	WC-GGA	This work
3.139	mBJ	This work
2.064	WC-GGA with SOI	This work
2.931	mBJ with SOI	This work
1.74	WC-GGA	[8]
2.13	EV-GGA	[8]
2.35	LDA	[15]
2.48	GGA	[15]
3.05	EV-GGA	[15]
3.13	mBJ	[15]

ones [23,28,29]. However, there are no experimental data in the literature for the band gap. The optical properties are band gap dependent; therefore we have selected the mBJ for further explanation of these properties. The spin-orbit interaction (SOI) has been also considered for the electronic properties calculations and the results are compared to those of non-SOI calculations. The calculated band structure (as prototype) using mBJ with SOI is displayed in Fig. 3, *c*. The spin-orbit interaction causes splitting of bands, resulting in the reduction of the band gap energy. The values obtained for the band gap with SOI are smaller than the non-SOI ones (Table 2). However, no significant influence of the spin-orbit interaction (SOI) is noted on the band gap energy, since the difference in the values obtained with SOI and non-SOI is very small. The composition and origin of bands can further understand by performing calculations of total and partial density of states. Using mBJ approximation, the total and partial density of states (TDOS and PDOS) corresponding to the band structure in Fig. 3 are illustrated in Fig. 4. The valence band below the Fermi level (E_F) consists of two regions, the lower part ranging from -10.96 eV to -9.48 is composed mainly by chalcogen s-states with a small contribution of s-Al and p-Al states. The higher one, ranges from -5.22 eV to Fermi level (0.0 eV), in this region, the main contribution comes from p-Al, p-Te and s-Al states as well as smaller contribution from p-Li and s-Li states. The conduction band consists essentially of p-Li, s-Li, s-Al and p-Al states. The calculated total and partial density of states (TDOS and PDOS) using WC-GGA approximation and including spin-orbit interaction is shown

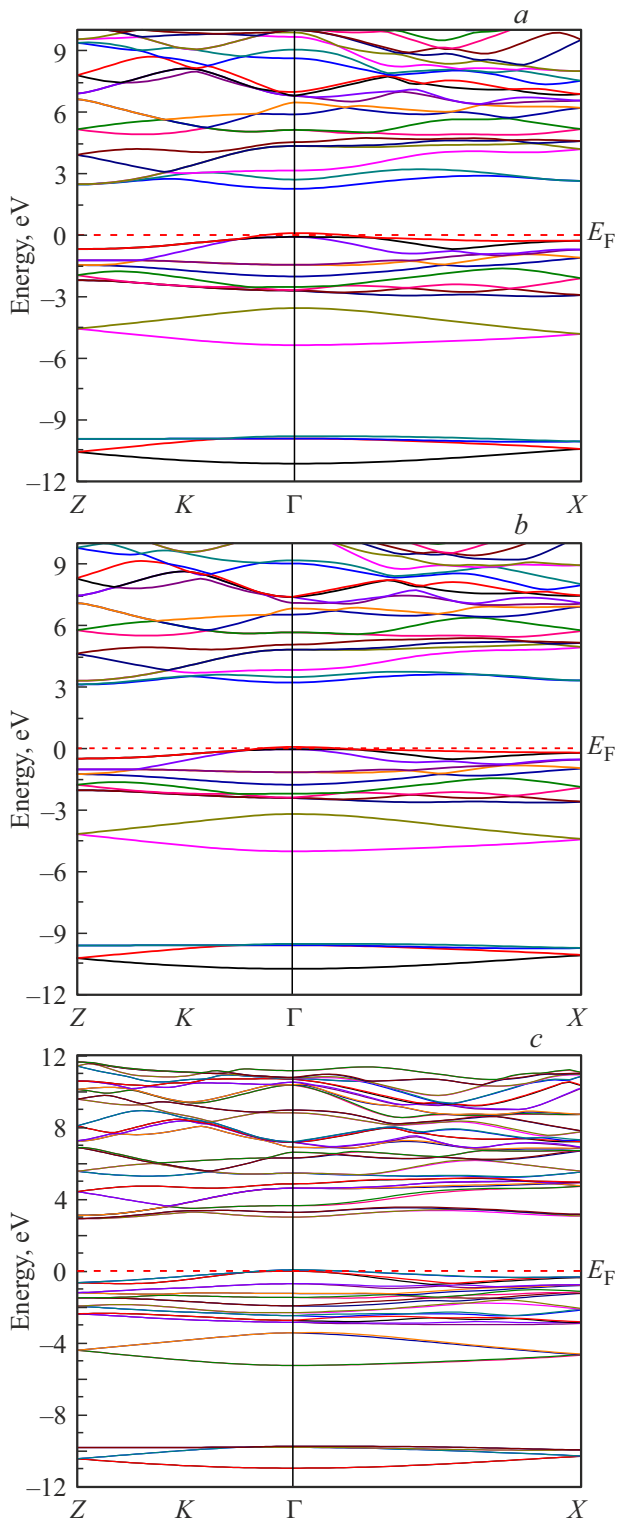

Figure 3. Calculated band structure of $LiAlTe_2$ (a) using WC-GGA (b) using mBJ and (c) using mBJ with SOI.

in Fig. 4, b. From this figure, it is clear that no changes in the contribution of the different orbitals are observed. Furthermore, the inclusion of spin-orbit interaction effects in the density of state calculations, induces only little changes in the band gap and in energy ranges of the different regions of the valence and conduction bands.

3.3. Optical properties

We now consider the optical properties for $LiAlTe_2$. The knowledge of the optical properties is crucial to understand the optoelectronics behavior of a material. The optical properties of a solid are described by the frequency-dependent complex dielectric function which is given by the following relation:

$$\varepsilon(\omega) = \varepsilon_1(\omega) + i\varepsilon_2(\omega) \tag{1}$$

where $\varepsilon_1(\omega)$ and $\varepsilon_2(\omega)$ represent the real and imaginary parts of the dielectric function, respectively. The real part $\varepsilon_1(\omega)$ is directly related to the refractive properties and the imaginary part $\varepsilon_2(\omega)$ determines the absorption spectrum. The imaginary part can be obtained from momentum matrix elements between the occupied and unoccupied electronic states [30]. The real part $\varepsilon_1(\omega)$ can be calculated from the imaginary part $\varepsilon_2(\omega)$ by using Kramers–Kronig relation [31]. The other optical properties such as the refractive index $n(\omega)$, the absorption coefficient $\alpha(\omega)$, and the reflectivity $R(\omega)$ can be evaluated from the complex dielectric function [32,33]. They are given by the following expressions:

$$n(\omega) = \left[\frac{\sqrt{\varepsilon_1^2(\omega) + \varepsilon_2^2(\omega)} + \varepsilon_1(\omega)}{2}\right]^{1/2}, \tag{2}$$

$$\alpha(\omega) = \sqrt{2}\omega\left[\sqrt{\varepsilon_1^2(\omega) + \varepsilon_2^2(\omega)} - \varepsilon_1(\omega)\right]^{1/2}, \tag{3}$$

$$R(\omega) = \left|\frac{\sqrt{\varepsilon(\omega)} - 1}{\sqrt{\varepsilon(\omega)} + 1}\right|^2. \tag{4}$$

For the tetragonal unit cell structure, the optical properties have been calculated along two different directions of polarization, extraordinary ($E \parallel c$ axis) and ordinary ($E \perp c$ axis). We display only the calculations according to the mBJ approximation because of the enhanced band-gap values.

The calculated real part of dielectric function for the studied compound is shown in Fig. 5 in an energy range of 0 −25 eV. From this figure, it is important to note that this compound exhibits isotropic behavior at high energies (beyond 10 eV). The most important quantity is the zero frequency limit $\varepsilon_1(0)$ which represents the electronic part of the static dielectric constant and it depends strongly on the band gap on the basis of Penn's model [34]. The mBJ results of static dielectric constant are listed in Table 3 and compared to previous theoretical works. From zero frequency, $\varepsilon_1(\omega)$ starts increasing and reaches the maximum values 12.254 (at 3.632 eV) and 11.405 (at 3.741 eV) for $\varepsilon_1^{\parallel}(\omega)$ and $\varepsilon_1^{\perp}(\omega)$, respectively. After that, the spectra exhibit a steep decrease in the range between 3.632 and 6.051 eV for $\varepsilon_1^{\parallel}(\omega)$ and 3.741 and 5.972 for $\varepsilon_1^{\perp}(\omega)$. Above this becomes $\varepsilon_1(\omega)$ negative and reaches

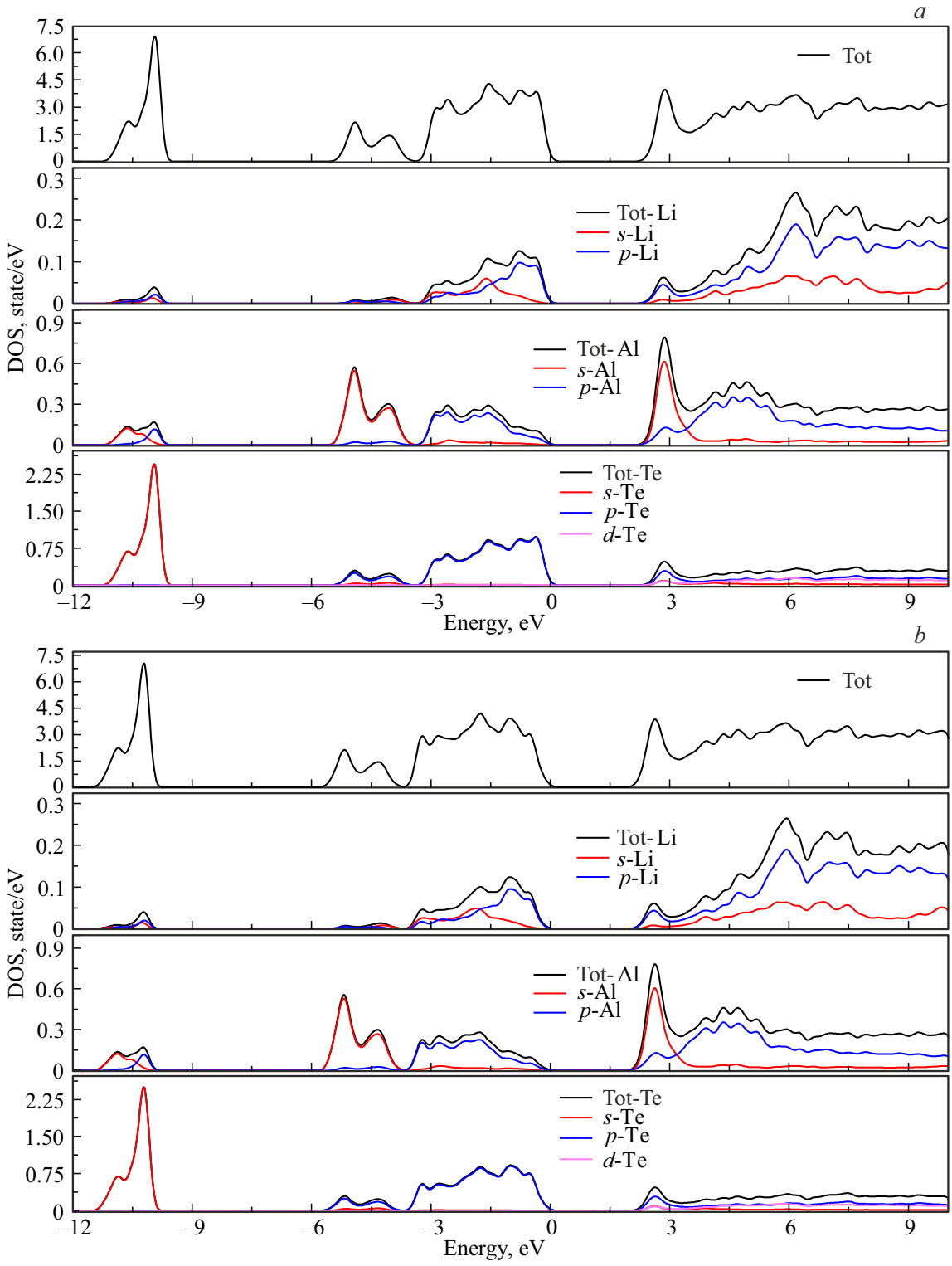

Figure 4. Total and partial densities of states of $LiAlTe_2$: (*a*) with no-SOI and (*b*) with SOI.

minimum values -3.219 (at 7.877 eV) and -2.201 (at 8.612 eV) for $\varepsilon_1^{\parallel}(\omega)$ and $\varepsilon_1^{\perp}(\omega)$, respectively, then $\varepsilon_1(\omega)$ slowly increases towards zero level at high energies. The anisotropy in real part $(\varepsilon_1^{\parallel}(\omega) - \varepsilon_1^{\perp}(\omega))$ is shown in Fig. 6. The maximum anisotropy peak (at 5.001 eV) occurs in the negative region. Moreover, $LiAlTe_2$ is practically anisotropic in the energy range less than 11.50 eV. From Table 3, it is noticed that the calculated static dielectric constants agree well with the results in Ref [15], the discrepancy with the values of Ref [14] is due to the use of the

LDA in this work which is known to underestimate the band gap.

The imaginary part of dielectric function is depicted in Fig. 7. The threshold energy appears at 3.159 eV which reflects the fundamental absorption edge and it is associated to the direct optical transitions between highest valence bands and lowest conduction bands at Γ point. By identification to the calculated electronic band structure, the threshold energy is closely related to the calculated mBJ band gap value. Beyond this point, the curve increases rapidly. This is due to the fact that the number of points contributing towards $\varepsilon_2(\omega)$ increases abruptly and consequently more interband transitions are present. The absorption region of $LiAlTe_2$ is in the energy range 3.15–10.30 eV. There are two main peaks for $\varepsilon_2^{\parallel}(\omega)$ and $\varepsilon_2^{\perp}(\omega)$ located at 4.911 eV and 5.428 eV, respectively (the maximum peak). The maximum anisotropy peak (at 4.83 eV) occurs in the positive region.

Another important quantity that we calculated is the refractive index $n(\omega)$ which is an important parameter in optical properties. The plot of refractive index is displayed in Fig. 8. From this figure, the static values of refractive index are 2.396 ($n^{\parallel}(0)$) and 2.370 $n^{\perp}(0)$, they are illustrated in Table 3 along with other calculated values. These findings are in favourable agreement with those of Ref [15] and are slightly lower compared to the results in Ref [8]. Beyond the zero frequency limit, the refractive index increases to a maximum value in the visible region and finally decreases with the further increase in energy until it evolves below the unit value ($n(\omega) < 1$) in the ultraviolet region. In this region, the phase velocity of the photon is greater than the speed of light c. However, the relativity relation is not affected because the group velocity in this region is always smaller than the speed of light. At high energy region (> 12 eV), the values of refractive index are very small even close to zero. The results suggests that for the high frequency electromagnetic wave, the absorption is very weak, and refractive index is almost constant at high frequency area, indicating that the $LiAlTe_2$ is transparent in the ultraviolet region. The birefringence $\Delta n(0)$ has been also estimated, it is given by the following relation [35]:

$$\Delta n(0) = n_e - n_o \tag{5}$$

where n_e and n_o respectively denote the extraordinary and ordinary refractive index and represent respectively $n^{\parallel}(0)$

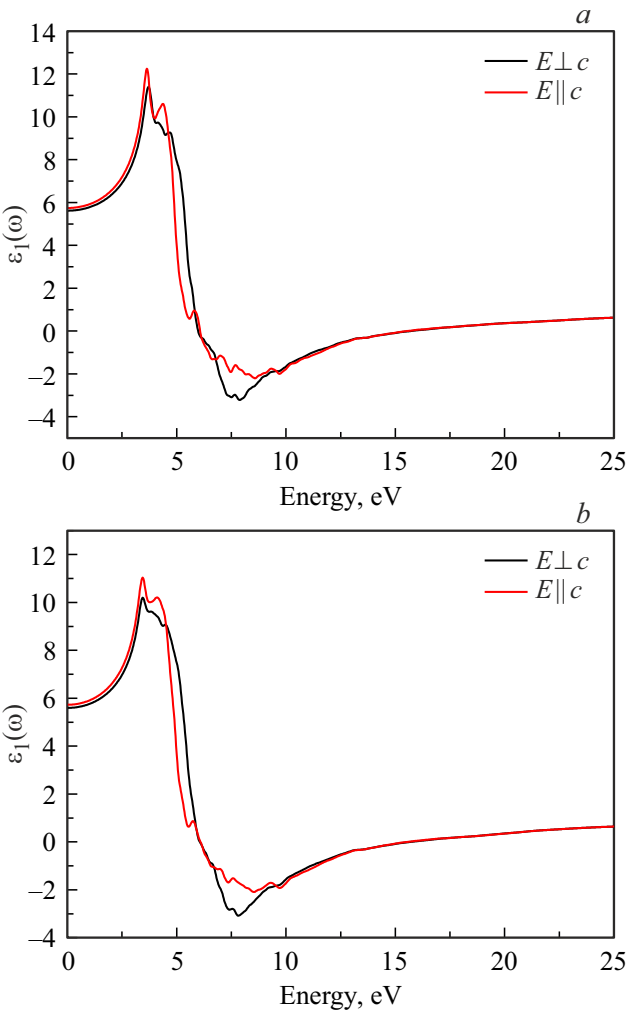

Figure 5. Real part of dielectric function $\varepsilon_1(\omega)$ as a function of energy for $LiAlTe_2$ compound: (a) with no-SOI and (b) with SO.

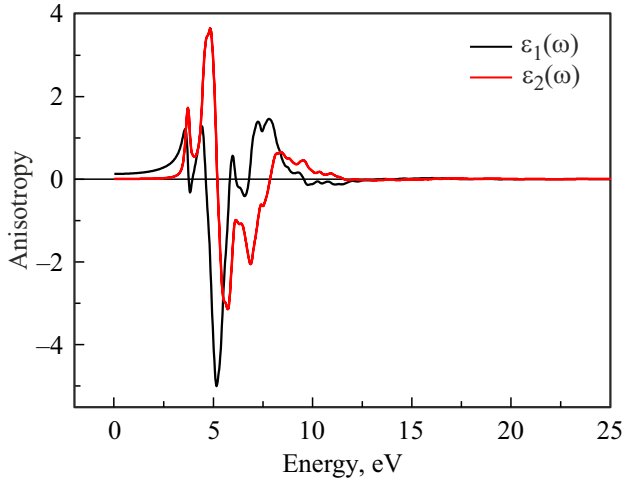

Figure 6. Calculated anisotropy in real and imaginary parts of dielectric function for $LiAlTe_2$ compound.

Table 3. Calculated static values of the dielectric function $\varepsilon(0)$, refractive index $n(0)$ and reflectivity $R(0)$ as well as the birefringence $\Delta n(0)$ of $LiAlTe_2$ compound

$\varepsilon_1^{\perp}(0)$	$\varepsilon_1^{\parallel}(0)$	$n^{\parallel}(0)$	$n^{\perp}(0)$	$\Delta n(0)$	$R^{\parallel}(0)$	$R^{\perp}(0)$
5.619[a]	5.744[a]	2.396[a]	2.370[a]	0.026[a]	0.169[a]	0.165[a]
5.610[b]	5.742[b]	2.396[b]	2.368[b]	0.028[b]	0.169[b]	0.165[b]
5.39[c]	5.45[c]	2.33[c]	2.32[c]	0.07[d]	0.192[e]	0.182[e]
6.59[c]	6.48[d]	2.565[e]	2.490[e]			

Note [a] This work, [b] This work with SOI, [c] Ref [15], [d] Ref [14], [e] Ref [8]

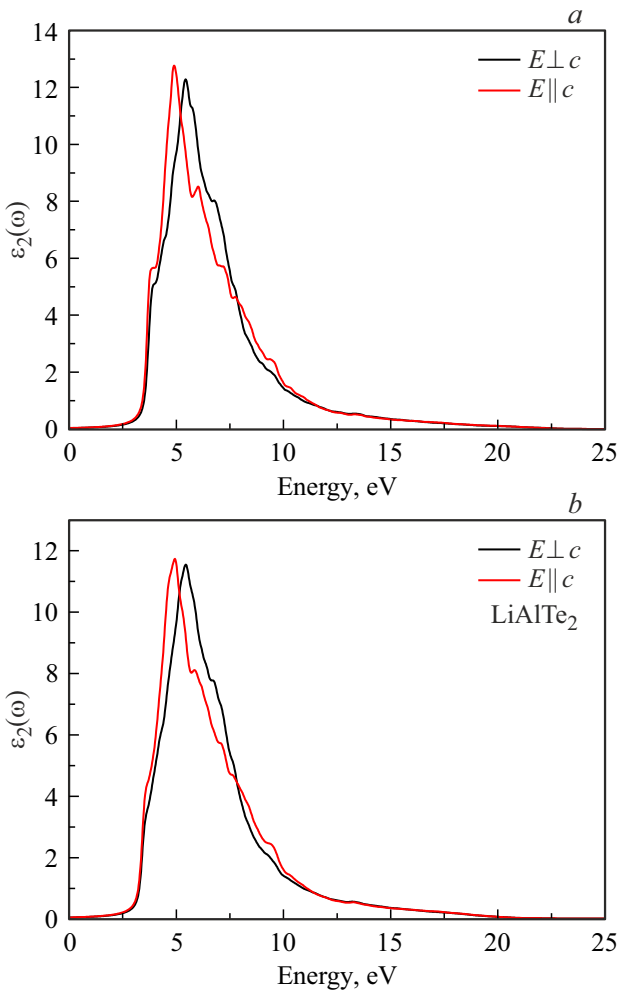

Figure 7. Imaginary part of dielectric function $\varepsilon_2(\omega)$ as a function of energy for $LiAlTe_2$ compound: (a) with no-SOI and (b) with SO.

and $n^{\perp}(0)$. The obtained value of birefringence is positive (Table 3), so the $LiAlTe_2$ compound is a positive uniaxial material. Birefringence is important only in the non-absorbing region, which is below the energy gap.

The optical reflectivity is displayed in Fig. 9. The static values of reflectivity which are depicted in Table 3 are in reasonable agreement with that obtained by Amjad Khan *et al* [8], the small difference is due to the used functional of the exchange-correlation potential. These materials have small reflectivity in the low energy range and a weak anisotropy is observed between the two components ($R^{\parallel}(0)$ and $R^{\perp}(0)$), $\Delta R(0) = 0.003$. The maximum reflectivity of this compound occurs in the energy range between 4.50 and 14.0 eV, which is in the ultraviolet region; thus this compound can be used as shields for ultraviolet radiations. The maximum reflectivity values are 51.5% and 50.3% for $R^{\parallel}(0)$ and $R^{\perp}(0)$, respectively. These values agree well with those of Ref [8] which are 48% and 46% for $R^{\perp}(\omega)$ and $R^{\parallel}(\omega)$, respectively. The absorption coefficient $\alpha(\omega)$ is a parameter, which indicates the fraction of light lost by the electromagnetic wave when it passes through a unit thickness of the material. It has been plotted in Fig. 10 for $LiAlTe_2$ compound. The absorption spectrum

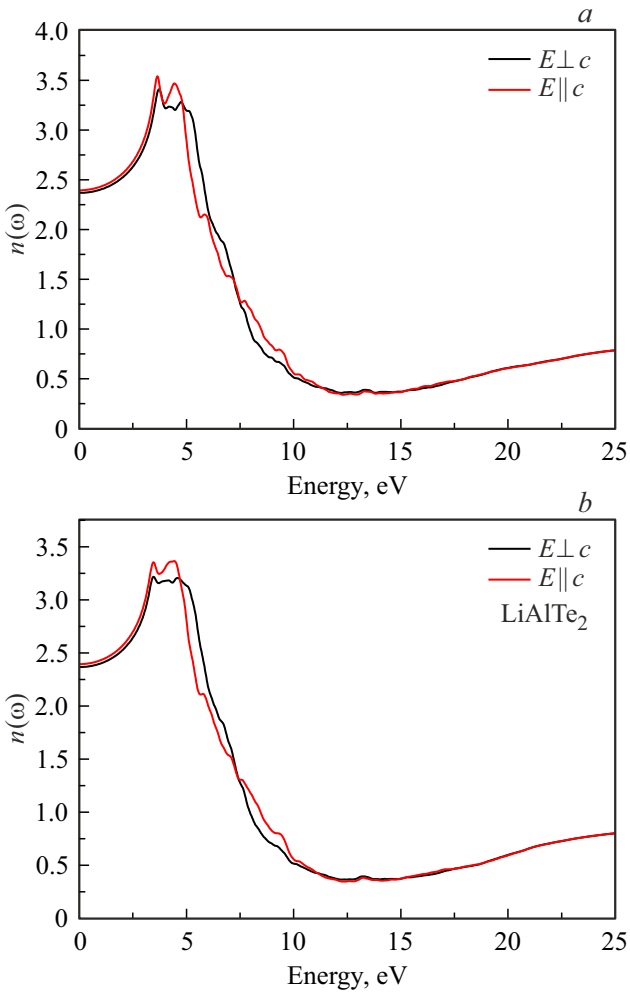

Figure 8. Refractive index $n(\omega)$ as a function of energy for $LiAlTe_2$ compound.

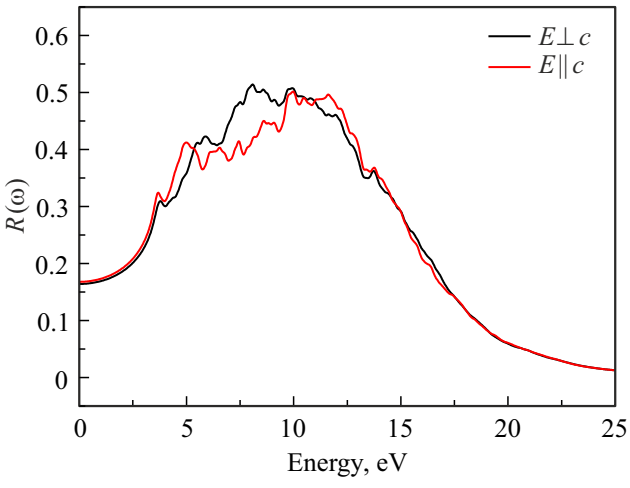

Figure 9. Reflectivity $R(\omega)$ as a function of energy for $LiAlTe_2$ compound.

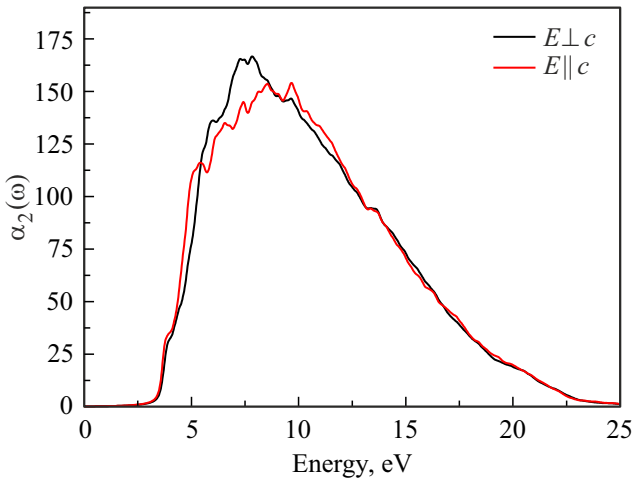

Figure 10. Absorption coefficient $\alpha(\omega)$ as a function of energy for $LiAlTe_2$ compound.

shows that the absorption edge is located at 3.115 eV which corresponds to its band gap value predicted by mBJ approximation. Beyond the absorption edge value, the absorption coefficient $\alpha(\omega)$ increases. According to figure 10, the maximum value of the absorption coefficient occurs at the energies 7.850 eV and 9.673 eV for $\alpha^{\perp}(\omega)$ and $\alpha^{\|}(\omega)$, respectively. The absorption coefficient further decreases rapidly in the high energy region, which is the typical characteristic of semiconductors.

The optical properties have been also calculated by including the spin-orbit interaction (SOI) since these properties are band gap dependent. As prototypes, we have displayed in Figs. 5, *b*, 7, *b* and 8, *b*, the calculated real part of dielectric function $\varepsilon_1(\omega)$, the imaginary part of dielectric function $\varepsilon_2(\omega)$ and the refractive index $n(\omega)$. The SOI has a negligible effect on the optical properties; the profiles of the obtained curves with SOI are similar to those obtained without SOI. This can be seen in table 3 where the calculated static optical parameters including SOI are almost identical to those calculated without SOI.

3.4. Thermal properties

To investigate the thermal properties of the $LiAlTe_2$ compound under higher temperature and pressure we have used Gibbs program [36] which is based on the „quasi-harmonic Debye model". The obtained set of total energy versus primitive cell volume determined in previous section has been used to derive macroscopic properties as a function of pressure and temperature from the standard thermodynamic relations. Gibbs function $G^*(V;P,T)$ for non-equilibrium conditions can be written in the form:

$$G^*(V;P,T) = E(V) + PV + A_{vib}[\theta(V;T)] \qquad (6)$$

where $E(V)$ is the total energy per unit cell, PV corresponds to the constant hydrostatic pressure condition, $\theta(V)$ is the Debye temperature and A_{vib} is the vibrational term. The vibrational part A_{vib} is computed from the phonon density of states of the material by employing the Debye model and can be expressed as given in the following expression [37,38]:

$$A_{vib}(\theta, T) = nk_{\mathrm{B}}T\left[\frac{9\theta}{8T} + 3\ln\left(1 - e^{-(\theta/T)} - D\left(\frac{\theta}{T}\right)\right)\right]. \qquad (7)$$

Where n and $D\left(\frac{\theta}{T}\right)$ are the number of atoms per formula unit and the Debye integral, respectively, for an isotropic solid, the Debye temperature is expressed as [37]:

$$\theta_D = \frac{\hbar}{k_{\mathrm{B}}}\left[6\pi^2 V^{1/2} n\right]^{1/3} f(\sigma)\sqrt{\frac{B_S}{M}}. \qquad (8)$$

Where B_S and M represent the adiabatic bulk modulus and molecular mass per unit cell, respectively, B_S is approximated by the static compressibility as [36]:

$$B_S \cong B(V) = V\left\{\frac{d^2E(V)}{dV^2}\right\}. \qquad (9)$$

The function $f(\sigma)$ is given by the following relation [36,39]:

$$f(\sigma) = \left\{3\left[2\left(\frac{21+\sigma}{31-2\sigma}\right)^{3/2} + \left(\frac{11+\sigma}{31-\sigma}\right)^{1/2}\right]^{-1}\right\}^{1/3} \qquad (10)$$

where σ denotes to Poisson ratio which is equal to 0.25 [40]. Therefore the non-equilibrium Gibbs function $G^*(V;P,T)$ as the function of $(V;P,T)$ can be minimized with respect to volume V:

$$\left[\frac{\partial G^*(V;P,T)}{\partial V}\right]_{P,T} = 0. \qquad (11)$$

We can obtain the thermal equation of state (EOS) $V(P,T)$ by determining the solution of equation (11). The expressions for isothermal bulk modulus (B_T), specific heat capacity (C_V) and entropy S are given in the followings [36]:

$$B_T(P,V) = V\left(\frac{\delta^2 G^*(V;P,T)}{\partial V^2}\right)_{P,T} \qquad (12)$$

$$C_V = 3nk_{\mathrm{B}}\left[4D\left(\frac{\theta}{T}\right) - \frac{3\theta/T}{e^{\theta/T}-1}\right] \qquad (13)$$

$$S = nk\left[4D\left(\frac{\theta}{T}\right) - 3\ln\left(1 - e^{-\theta/T}\right)\right]. \qquad (14)$$

Through the quasi-harmonic Debye model, we have calculated thermal parameters of any temperatures and pressures of the studied compound from the calculated $E-V$ data at $T = 0$ and $P = 0$. The thermal properties are determined in the temperature range from 0 to 1000 K and pressure effects are studied in 0–8 GPa range.

The variations of the cell volume and bulk modulus with temperature at various pressures are illustrated in Fig. 11 (*a*) and (*b*). From figure 11,(*a*), one can see that at a fixed pressure, the volume increases slightly as the

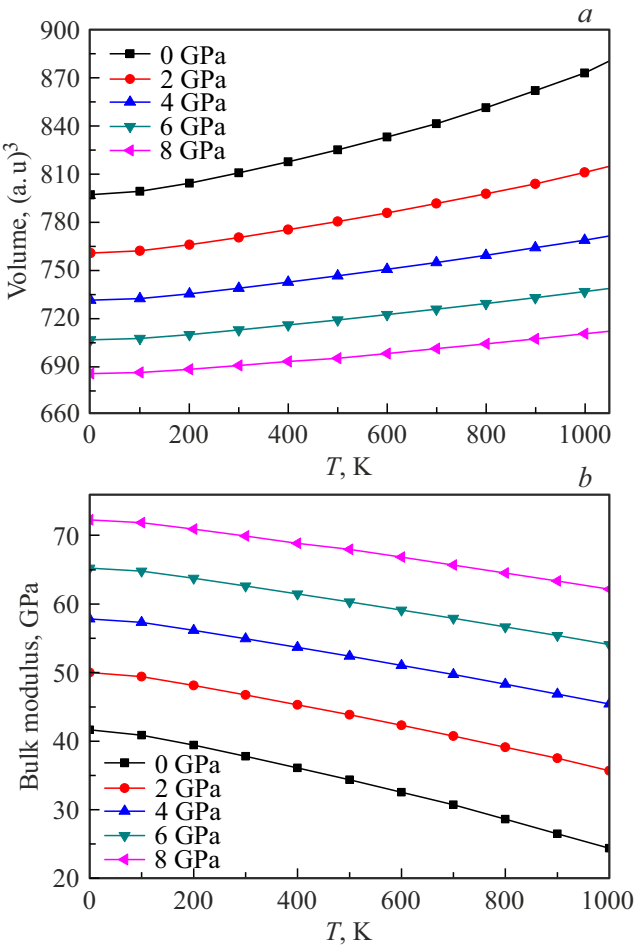

Figure 11. Variation of volume (a) and bulk modulus (b) as a function of temperature at various pressures for $LiAlTe_2$ compound.

temperature increases while at a given temperature, the volume decreases dramatically as the pressure increases. This indicates that the temperature and pressure have inverse effects; an increase in temperature leads to an expansion in the crystal and an increase in pressure reduces this effect. The bulk modulus is nearly constant from 0 to 100 K (Fig. 11 (b)) and beyond this temperature value, the bulk modulus decreases with increasing temperature when the pressure is fixed. This means that the compressibility of the crystal increases with rising the crystal's temperature at a given pressure. Also increasing the pressure at a given temperature decreases the compressibility of the crystal. The ability to resist the volume change becomes stronger when the pressure increases. The cell volume and bulk modulus values for simulated crystalline ($T = 300$ K an $P = 0$ GPa) are 810.86 (a.u)^3 and 34.80 GPa, respectively.

The Debye temperature θ_D is an important fundamental parameter because it characterizes many physical quantities such as specific heat, melting temperature and hardness of the solids [41]. Fig. 12 represents the variation of the Debye temperature with the temperature at various pressures. As it can be seen, the Debye temperature is nearly constant from 0 to 100 K and decreases with the increase in temperature when $T > 100$ K. At a fixed temperature, the Debye temperature increases with increasing applied pressures.

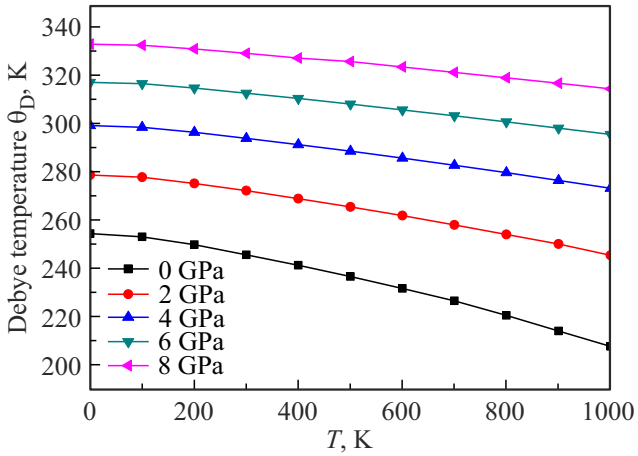

Figure 12. Variation of Debye temperature as a function of temperature at various pressures for $LiAlTe_2$ compound.

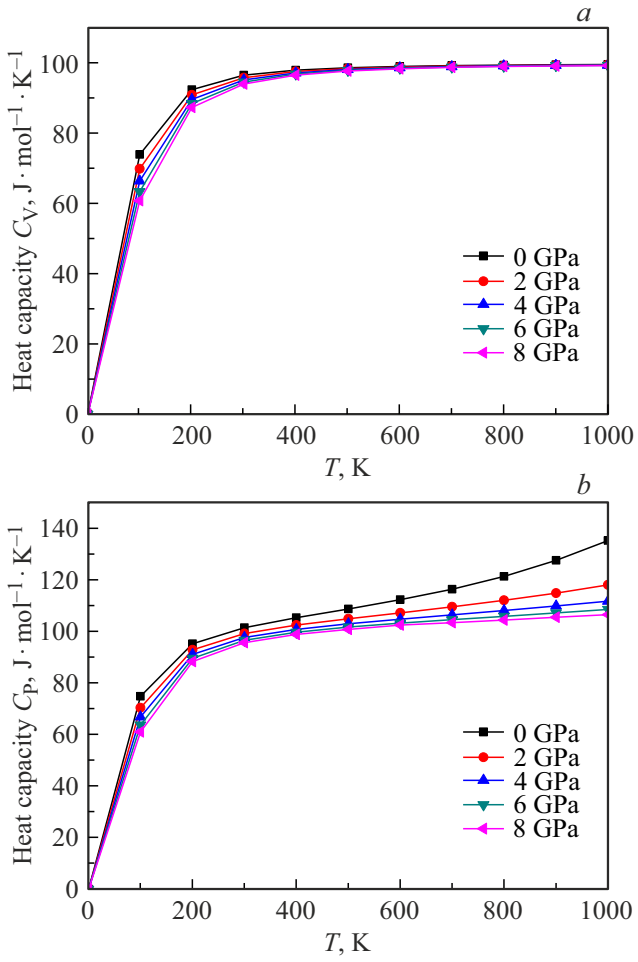

Figure 13. Variation of heat capacity C_V (a) and heat capacity C_P (b) as a function of temperature at various pressures for $LiAlTe_2$ compound.

This behavior can be explained by the fact that Debye temperature is proportional to the bulk modulus and that a hard material exhibits a high Debye temperature. Our calculated value of the θ_D ($T = 300$ K and $P = 0$ GPa) is 245.65 K.

The heat capacities at constant volume C_V and constant pressure C_P of any crystalline material not only describe the vibrational properties but are required for many applications. The calculated heat capacities C_V and C_P of $LiAlTe_2$ versus temperature at pressure range 0−8 GPa are displayed in Fig. 13 (*a*) and (*b*), respectively. From these figures, at low temperatures C_V and C_P adopt similar behavior; both of them are proportional to T^3 [42] but with no appreciable variation with pressure. With increasing temperature, C_V tends progressively to the classical Dulong–Petit limit of $3nR = 12R$ (99.77 J/mol K) [43] whereas C_P increases monotonically. It is noted that the effect of pressure is more remarkable on C_P than on C_V. The predicted values of C_V and C_P ($T = 300$ K and $P = 0$ GPa) are 96.507 J/mol K and 101.424 J/mol K, respectively. To the best of our knowledge, neither measurements nor theoretical calculations of thermal properties of this compound are available in the literature.

4. Conclusions

In the present study, the structural, electronic, optical and thermal properties of $LiAlTe_2$ compound in chalcopyrite structure are calculated using the FP-LAPW method as framed within DFT formalism. For the structural parameters, a reasonable agreement with other available theoretical and experimental results has been found. The computation of the band gap using WC-GGA and mBJ shows that this compound is direct band gap (Γ-Γ) semiconductor. Our band gap value is very close to previous theoretical findings. The optical properties of the studied compound have been analysed in order to reveal optoelectronic utilities. The optical quantities such as real and imaginary parts of the dielectric function, the refractive index, the reflectivity, the absorption coefficient and the birefringence were determined for energies ranging from 0 eV to 25 eV. At low energies, it is observed that the dielectric function and refractive index, as well as other important optical properties are nearly anisotropic which makes this compound very useful for various linear-nonlinear optical devices. The static values of dielectric function and refractive index are consistent with available data. Thermal quantities such as unit cell volume, bulk modulus, Debye temperature and heat capacities are calculated at various temperatures and pressures based on the quasi-harmonic Debye model. Hence it would be beneficial to verify experimentally the predicted results which will hope to stimulate the succeeding studies.

Acknowledgments

The authors acknowledge the financial Support of the General Direction of Scientific Research and Technological Development (DGRSDT).

Conflict of interest

The authors declare that they have no conflict of interest.

References

[1] B.H. Bairamov, A. Aydinli, I.V. Bodnar, Y.V. Rud, V.K. Nogoduyko, and V.V. Toporov, J. Appl. Phys. **80**, 5564 (1996).
[2] H.S. Saini, M. Singh, A.H. Reshak, and M.K. Kashyap, J. Alloys Compd. 518, 74 (2012)
[3] S. Ullah, G. Murtaza, R. Khenata, and A.H. Reshak, Mat. Sci. Semicon. Proc. **26**, 79 (2014).
[4] V.L. Shaposhnikov, A.V. Krivosheeva, V.E. Borisenko, J.-L. Lazzari, and F. Arnaud d'Avitaya, Phys. Rev. B **85**, 205201 (2012).
[5] J.Y. Kim, and T. Hughbanks, Inorg. Chem. **39**, 3092 (2000).
[6] Y.E. Romanyuk, L.P. Marushko, L.V. Piskach, I.V. Kityk, A.O. Fedorchuk, V.I. Pekhnyo, and O.V. Parasyuk, Cryst. Eng. Commun. **15**, 4838 (2013).
[7] G.P. Gorgut, A.O. Fedorchuk, I.V. Kityk, V.P. Sachanyuk, I.D. Olekseyuk, and O.V. Parasyuk, J. Cryst. Growth **324**, 212 (2011).
[8] Amjad Khan, M. Sajjad, G. Murtaza, and A. Laref, Z. Naturforsch, **1** (2018).
[9] L.L. Kazmerski, Il. Nuovo Cimento D **2**, 2013 (1983).
[10] S. Ozaki, and S. Adachi, J. Appl. Phys. **100**, 113526 (2006).
[11] I.G. Vasilyeva, R.E. Nikolaev, P.G. Krinitsin, and L.I. Isaenko, J. Phys. Chem. C **121**, 17429 (2017).
[12] F.K. Hopkins, Laser Focus World **31**, 87 (1995).
[13] A.V. Kosobutsky, Yu.M. Basalaev, and A.S. Poplavnoi, Phys. Status Solidi B **246**, 364 (2009).
[14] A.V. Kosobutsky, and Yu.M. Basalaev J. Phys. Chem. Solids. **71**, 854 (2010).
[15] A.H. Reshak, and Wilayat Khan, J. Alloys Compd.592, **92** (2014).
[16] L. Isaenko, P. Krinitsin, V. Vedenyapin, A. Yelisseyev, A. Merkulov, J.-J. Zondy, and V. Petrov, Cryst. Growth Des. **5**, 1325 (2005).
[17] V. Petrov, L. Isaenko, A. Yelisseyev, P. Krinitsin, V. Vedenyapin, A. Merkulov, and J.-J. Zondy, J. Non-Cryst. Solids **352**, 2434 (2006).
[18] O.K. Andersen. Phys. Rev. B **42**, 3063(1975).
[19] P. Hohenberg, and W. Kohn, Phys. Rev. B **136**, 864 (1964).
[20] W. Kohn, and L.J. Sham, Phys. Rev. **140**, A1133 (1965).
[21] P. Blaha, K. Schwarz, G. K.H. Madsen, D. Kvasnicka, and J. Luitz, WIEN2k. An Augmented Plane Wave + Local Orbitals Program for Calculating Crystal Properties Vienna University of Technology, (Vienna, Austria, 2001).
[22] Z. Wu, and R.E. Cohen, Phys. Rev. B **73**, 235116 (2006).
[23] F. Tran, and P. Blaha, Phys. Rev. Lett. **102**, 226401 (2009).
[24] A.D. Becke, and E.R. Johnson, J. Chem. Phys. **124**, 221101 (2006).
[25] H.J. Monkhorst, and J.D. Pack, Phys. Rev. B **13**, 5188 (1976).
[26] F.D. Murnaghan. Proc. Natl. Acad. Sci. USA **30**, 244 (1947).
[27] L. Isaenko, I. Vasilyeva, A. Merkulov, A. Yelisseyev, and S. Lobanov, J. Cryst. Growth **275**, 217 (2005).
[28] D.J. Singh. Phys. Rev. B **82**, 155145 (2010).
[29] D.J. Singh. Phys. Rev. B **82**, 205102 (2010).
[30] M. Gajdoš, K. Hummer, G. Kresse, J. Furthmüller, and F. Bechstedt, Phys. Rev. B **73**, 045112 (2006).
[31] R. de L. Kronig. J. Opt. Soc. Am. B **12**, 547 (1926).

[32] J. Sun, H. Wang, J. He, and Y. Tian, Phys. Rev. B **71**, 125132 (2005).
[33] S. Ozaki, and S. Adachi, J. Appl. Phys. **75**, 7470 (1994).
[34] D.R. Penn. Phys. Rev. **128**, 2093 (1962).
[35] N. Seddiki, T. Ouahrani, L. Boumediene, T. Benouaz, A.H. Reshak, and B. Bouhafs, Mat. Sci. Semicon. Proc. **16**, 1454 (2013).
[36] M.A. Blanco, E. Francisco, and V. Luaña, Comput. Phys. Commun. **158**, 57 (2004).
[37] M.A. Blanco, A. Martín Pendàs, E. Francisco, J.M. Recio, and R. Franco, J. Mol. Struct. Theochem **368**, 245 (1996).
[38] M. Florez, J.M. Recio, E. Francisco, M.A. Blanco, and A. Martìn Pendàs, Phys. Rev. B **66**, 144112 (2002).
[39] E. Francisco, M.A. Blanco, and G. Sanjurjo, Phys. Rev. B **63**, 094107 (2001).
[40] J.P. Poirier. Introduction to the Physics of the Earth's Interior, Cambridge University Press, Oxford 39.
[41] V. Kanchana, G. Vaitheeswaran, A. Svane, and A. Delin, J. Phys.: Condens. Matter **18**, 9615 (2006).
[41] P. Debye. Ann. Phys. **344**, 789 (1912)
[42] A.T. Petit, and P.L. Dulong, Ann. Chim. Phys. **10**, 395 (1819)